CrystEngComm

PAPER

View Article Online
View Journal | View Issue

Cite this: *CrystEngComm*, 2026, **28**, 2670

A kinetically informed thermodynamic (KIT) design framework for understanding the crystallization characteristics of resveratrol

Monika Neal, [a] Álmos Orosz,[ab] Rekha Rao[c] and Zoltan K. Nagy *[a]

Crystallization is a crucial process in the production of solid materials across various industries, where it not only purifies the compound but also defines essential particle attributes. These particle-specific critical quality attributes (CQAs), including crystal size distribution, morphology, and purity, directly impact the quality and efficiency of downstream operations, such as filtration, drying, and formulation. The ability to precisely control these attributes during crystallization is essential for ensuring consistent product quality, process efficiency, and regulatory compliance. Many process parameters can influence CQAs; the solvent is often the first variable investigated when designing a crystallization process, and selection is typically guided by thermodynamic criteria such as solubility and theoretical yield. However, as development advances to larger scales, kinetic limitations such as agglomeration or poor crystal habit often emerge, driven by factors like local supersaturation, mixing inefficiencies, and particle–particle interactions. These behaviors are difficult to predict from solubility data alone and require experimental insight to effectively manage. This study presents a kinetically informed thermodynamic (KIT) design framework for solvent screening to help mitigate these issues. The KIT design framework enhances early decision-making by combining traditional thermodynamic screening with straightforward kinetic assessments using small-scale cooling crystallization experiments. Through qualitative observations of nucleation, growth, agglomeration, and aspect ratio, the framework helps prioritize solvents that not only meet yield targets but also support desirable kinetic behavior. This integrated approach improves the reliability of solvent selection, reduces the likelihood of scale-up challenges, and minimizes the need for extensive late-stage process troubleshooting.

Received 14th July 2025,
Accepted 15th March 2026

DOI: 10.1039/d5ce00702j

rsc.li/crystengcomm

1. Introduction

Crystallization is often the final stage in active ingredient production and has a direct impact on product purity, process yield, and downstream handling.[1–3] The resulting crystal properties, such as crystal size distribution (CSD), shape, and purity, are considered critical quality attributes (CQAs) and influence manufacturability aspects such as filtration efficiency, drying behavior, and formulation performance.[4,5] Despite its widespread use, crystallization remains a complex and highly sensitive process, influenced by many critical process parameters, including solvent choice, seed load, and temperature or antisolvent addition profile. Small deviations in these conditions can lead to undesired outcomes such as uncontrolled nucleation, poor reproducibility, agglomeration, or the formation of unintended polymorphs.[6,7] Therefore, achieving robust and scalable crystallization processes requires a thorough understanding of both thermodynamic (*e.g.*, solubility and yield) and kinetic (*e.g.*, nucleation and growth rates) factors.[8]

To address these challenges, frameworks such as quality-by-design (QbD) and quality by control (QbC) have been developed. QbD emphasizes systematic process development using tools like design of experiments (DoE) and process analytical technology, while QbC introduces dynamic feedback control strategies to guide crystallization in real time.[9–12] Within QbC, direct nucleation control (DNC) is a prominent model-free approach that adjusts temperature dynamically based on real time PAT data such as particle count or turbidity. This closed-loop control introduces temperature cycling, which has been shown to reduce agglomeration, increase crystal size, and narrow the CSD.[2,11,13,14–16] However, despite advances in control strategies, early-stage solvent selection is primarily guided by thermodynamic properties such as solubility and theoretical yield. While solvents that exhibit high solubility variation between temperatures are often favored for cooling crystallization, this approach overlooks critical kinetic factors,

[a] *Davidson School of Chemical Engineering, Purdue University, West Lafayette, IN, USA. E-mail: zknagy@purdue.edu*
[b] *Department of Chemical and Environmental Process Engineering, Faculty of Chemical Technology and Biotechnology, Budapest University of Technology and Economics, Műegyetem rkp. 3, Budapest H-1111, Hungary*
[c] *Sandia National Laboratories, Albuquerque, New Mexico 87185, USA*

which can lead to challenges during scale up, such as agglomeration, undesired crystal morphology, or poor nucleation and growth behavior.[17,18]

To address deficits in traditional solvent selection techniques, a kinetically informed thermodynamic (KIT) design framework was developed to incorporate early-stage kinetic insights into the small-scale solvent screening process.[19] The KIT approach enables a more holistic solvent selection while reducing the risk of scale-up failures due to poor kinetic performance by integrating qualitative initial kinetic and visual indicators observed through PAT tools. A detailed kinetic analysis was completed in a separate publication focusing on a single solvent system, allowing this work to concentrate on early-stage screening.[20]

In this study, the material of focus is resveratrol, or 5-[(*E*)-2-(4-hydroxyphenyl)ethen-1-yl]benzene-1,3-diol, due to its pharmaceutical relevance and the practical challenges it presents in crystallization, particularly in morphology control and agglomeration behavior.[21,22] The objective here is to systematically evaluate the effects of cooling rate and initial concentration across different solvents, using visual and kinetic indicators to guide identification of solvent systems with the most promising and controllable crystallization profiles for future process development.

2. Experimental materials and methods

2.1. Materials

Resveratrol (Fig. 1) was obtained from VWR International (Avantor), Radnor, PA, USA (purity 98%). Given the limited crystallization data available for resveratrol, a broad solvent screening was performed to evaluate its solubility behavior and crystallization potential. The solvents investigated included ethanol (EtOH, 100%), methanol (MeOH, HPLC grade), dimethyl sulfoxide (DMSO, ACS grade), acetonitrile (HPLC grade), cyclohexane (99%), 2-butanone (97%), ethyl acetate (HPLC grade), 2-butanol (99%), isopropanol (IPA, HPLC grade), water (HPLC grade), *n*-heptane (99%), tetrahydrofuran (THF, HPLC grade), *n*-propanol (certified ACS), and toluene (certified ACS) all procured from Themo Fisher Scientific.

2.2. Solubility screening using the KIT design approach

The KIT solvent selection process begins with collecting equilibrium solubility data at an elevated temperature (60 °C) and ambient temperature (20 °C). These studies were performed using the Technobis Crystalline, which allows for small-scale solubility screening with precise temperature control, controlled stirring, transmissivity measurements, and in-line imaging for qualitative visualization. For each solvent, 6 mL was dispensed into a vial and equilibrated at the target temperature before adding an excess amount of resveratrol to ensure saturation. The solutions were held at that temperature while mixing for 4 hours to allow sufficient time for saturation to be reached. Then, standard gravimetric analysis was completed, in which the saturated solutions were filtered to remove the undissolved solids, the known solvent amount was evaporated, and the remaining solute weight was used to calculate the solubility concentration. Evaluating the solvents at two temperatures allowed preliminary insight into the suitability of the solvent for further crystallization development, specifically enabling the calculation of key process-relevant metrics: theoretical yield, solid concentration, and process sustainability (*E*-factor), as well as regulatory classification.

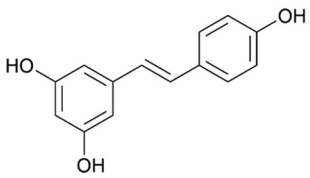

Fig. 1 Chemical structure of resveratrol.

Theoretical yield ($y_{\text{theoretical}}$, %) was calculated to understand the potential recovery of resveratrol during a cooling crystallization experiment:

$$y_{\text{theoretical}} = \left(\frac{c_{\text{high}} - c_{\text{ambient}}}{c_{\text{high}}}\right)\cdot 100 \quad (1)$$

where c_{high} and c_{ambient} are the dissolved resveratrol concentrations (mg $mL_{solvent}^{-1}$) at 60 °C and 20 °C, respectively. The solid concentration is important because if this value is too high, the viscosity of the slurry can make mixing more difficult, allowing for local supersaturation variation and increase:

$$\text{Solid concentration} = \left(\frac{(c_{\text{high}} - c_{\text{ambient}})\cdot 1000}{\rho_{\text{solvent}}}\right)\cdot 100 \quad (2)$$

where ρ_{solvent} is the density of the solvent (g mL^{-1}). The *E*-factor ($g_{solvent}\ g_{solute}^{-1}$) gives insight into the sustainability of the process:[23]

$$E = \left(\frac{\rho_{\text{solvent}}}{(c_{\text{high}} - c_{\text{ambient}})\cdot 1000}\right) \quad (3)$$

These thermodynamically derived parameters provide early insight into the feasibility and sustainability of each solvent system. Solvents exhibiting high theoretical yield and acceptable solid concentrations – indicative of favorable driving force and manageable processability – were selected for subsequent kinetic experiments. Their solubility data were fitted to a second-order polynomial of the form:

$$c_s = a\cdot T^2 + b\cdot T + c \quad (4)$$

where c_s is the solubility, T is the temperature (°C), and a, b, and c are the empirical fitting coefficients. Simple batch crystallization trials were conducted to qualitatively assess nucleation tendency, growth behavior, agglomeration, and crystal aspect ratio, offering an initial understanding of the kinetic behavior associated with each solvent. The integrated screening strategy balances thermodynamic potential with kinetic observability, facilitating more informed and efficient

solvent selection in the early stages of crystallization process development.

2.3. Crystallization design of experiments

Cooling crystallization experiments were run using a Mettler Toledo EasyMax 102, which offers precise control over temperature and agitation. Two solvent systems were selected for evaluation: (2 : 1 w/w, *i.e.*, weight-to-weight ratio) ethanol–water binary mixture and acetonitrile. These solvents were chosen based on the preliminary KIT design screening, which indicated favorable thermodynamic and kinetic characteristics. A design of experiments (DoE) was run for both solvents and is summarized in Table 1. For each cooling profile, three seed loads were evaluated: 0 wt% seed (unseeded), 1 wt% seed (low), and 5 wt% seed (high). Seeded experiments were conducted using raw resveratrol sieved through a 65 μm mesh to ensure consistent seed size. The same seed batch was used across all experiments requiring seeding and was introduced into the solution at 40 °C.

For (2 : 1) ethanol–water system, an initial concentration of 0.0774 g $g_{solution}^{-1}$ in 68 g of the ethanol–water mixture was used. The solution was first heated to 55 °C and held at that temperature for 1 hour under a stirring rate of 300 rpm to ensure complete dissolution. The solution was then cooled to a final temperature of 10 °C at two controlled linear cooling rates of 0.1 °C min^{-1} (slow) and 0.5 °C min^{-1} (fast). During cooling, seeding was performed, if required, as the system cooled and all solutions were held for 1 hour after reaching the 10 °C final temperature to allow for crystal equilibration.

For the acetonitrile system, a similar crystallization approach was followed. The initial concentration of 1.356 g was dissolved in 68 g of solvent. The solution was heated to 60 °C and held for 1 hour to ensure full dissolution. It was then cooled to 10 °C at the same two cooling rates (0.1 and 0.5 °C min^{-1}) and the same seed loads at a 300 rpm stirring rate. Each experiment was held at 10 °C for 1 hour after cooling.

All experiments were conducted under constant stirring using a standard three-blade impeller, and process analytical technology (PAT) tools were used to monitor crystallization behavior *in situ*. A Mettler-Toledo ParticleTrack G400 with a FBRM (focused beam reflectance measurement) probe was employed to observe changes in chord length distributions and overall particle counts, enabling detection of nucleation and growth trends, a Mettler-Toledo EasyViewer 100 probe provided high-resolution real-time imaging of crystal morphology, and a Hellma attenuated total reflection (ATR) probe connected to a Zeiss UV/vis spectrometer captured *in situ* spectral data of the solution.

Table 1 Design of experiments

	Seed load (wt%)	Cooling rate (°C min^{-1})
Experiment 1	0.0	0.1
Experiment 2	0.0	0.5
Experiment 3	1.0	0.1
Experiment 4	1.0	0.5
Experiment 5	5.0	0.1
Experiment 6	5.0	0.5

2.4. Direct nucleation control

In addition to linear cooling crystallization experiments, experiments were also conducted under closed-loop feedback control using a method known as direct nucleation control (DNC). This control strategy, as shown by Wu *et al.*, adjusts the temperature profile based on real-time process values collected through PAT tools, aiming to maintain a target level of particle counts or turbidity throughout the crystallization process.[14,24] In this approach, the desired number of particle counts or turbidity value (as measured by the FBRM in real-time) is predetermined based on prior experiments and design goals. If the measured value is below the target, indicating insufficient nucleation, the system automatically begins cooling, increasing supersaturation to promote nucleation. Conversely, if the particle count exceeds the target (indicating too much nucleation), the system begins heating to dissolve the fine particles and lower the counts. This feedback loop ensures the process remains within a desirable nucleation regime by alternating between two fixed temperature ramps (a cooling and a heating value). In doing so, DNC has also been shown to minimize agglomeration by maintaining more uniform and controlled population of crystals.[25] The DNC protocol was executed using in-house software, CryMoCo.[26] CryMoCo interfaces directly with the Mettler-Toledo EasyMax 102 reactor and the FBRM probe, enabling change in the temperature setpoint while reading the desired value from the FBRM.

Two DNC experiments were conducted for resveratrol in acetonitrile, as ethanol–water showed minimal agglomeration throughout the DoE. The setup mirrored that of the linear cooling crystallization experiments with a concentration of 16.95 mg mL^{-1} in the Mettler-Toledo EasyMax 102. The experiments both began at 60 °C and the temperature was adjusted based on real-time particle count data from the FBRM, using two predetermined temperature ramp rates: +0.3 °C min^{-1} for heating and 0.3 °C min^{-1} for cooling. The system switched between these two fixed rates based on whether the FBRM total particle count fell below or exceeded a specified target range. In the first experiment, the target range of particle counts was 3600–5400. In the second experiment, the target range was 1200–1600 total counts, however the solution was seeded 1 wt% resveratrol at 40 °C. Seeding was introduced to evaluate its influence on the particle size and morphology with the resulting temperature cycles.

2.5. Characterization

2.5.1. Raman. Offline samples of resveratrol crystals were analyzed using a Thermo-Fisher Scientific DXR Raman microscope to obtain the Raman spectra. In this analysis, individual single crystals were selected and measured directly

Table 2 Summary of crystallization feasibility and kinetic observations across solvent systems

	Solvent	Feasible	Nucleation	Growth	Agglomeration	Aspect ratio
1	Acetonitrile	Yes	High	High	Low	Low
2	Isopropanol	No	None	None	—	—
3	Ethanol	Yes	High	Low	Low	Low
4	Methanol	Yes	High	High	High	High
5	2-Butanol	No	None	None	—	—
6	*n*-Propanol	No	None	None	—	—
7	2-Butanone	No	None	None	—	—
8	Dimethyl sulfoxide	No	None	None	—	—
9	Ethyl acetate	No	None	None	—	—
10	Toluene	Insoluble	—	—	—	—
11	Water	Insoluble	—	—	—	—
12	Tetrahydrofuran	Insoluble	—	—	—	—
13	Ethanol–water (2 : 1)	Yes	High	High	Low	High
14	IPA–water	Yes	High	High	High	High
15	Acetonitrile–2-butanol	No	None	None	—	—
16	Acetonitrile–IPA	No	None	None	—	—
17	Cyclohexane–IPA	Insoluble	—	—	—	—
18	2-Butanol–water	Immiscible	—	—	—	—
19	THF–water	Immiscible	—	—	—	—

under the microscope to ensure high-resolution spectral data. The collected spectra were compared to the Raman spectrum of the raw material to confirm chemical identity of the product and assess consistency in solid-state form across different crystallization conditions. This analysis was used as a qualitative check to support observations of crystal morphology and process reproducibility.

2.5.2. UV/vis. Ultraviolet-visible (UV/vis) spectra of resveratrol in solution were collected during crystallization experiments using a Hellma attenuated total reflection (ATR) probe connected to a Zeiss UV/vis spectrometer. The ATR-UV/vis setup enabled *in situ*, real-time spectral acquisition without sample withdrawal and is well-suited for qualitative spectral analysis and quantitative concentration monitoring. To minimize baseline drift and improve resolution of key absorbance features, the first derivative of the spectra was applied during data processing.

3. Results and discussion

3.1. Solubility screening

The KIT design framework was implemented for preliminary solvent screening for crystallization of resveratrol. A broad range of solvent systems were evaluated, with the outcomes summarized in Table 2. The first screening criterion was the feasibility of crystallization in each solvent. Feasibility was defined as the occurrence of nucleation and growth during cooling crystallization, assessed visually *via* the Technobis Crystalline and categorized as either "high" or "low". Solvents were deemed unfeasible if no crystallization occurred ("none" under nucleation and growth), if resveratrol was insoluble in the solvent system, or if solvent mixture was immiscible. For those deemed feasible, observations of kinetic behavior were also recorded.

As a rapid yet informative understanding of solubility behavior, each solvent was evaluated at two temperatures, 20 °C and 60 °C; representative results for a subset of these solvents are shown in Fig. 2. Among the solvents, toluene and water exhibited the lowest solubilities, while ethanol and methanol showed the highest. These two solubility data points were used to estimate the theoretical yield, solid concentration, and *E*-factor, to provide a deeper understanding of each solvent's suitability for crystallization. These calculations, along with the solvent class, are summarized in Table 3. The solvent class is a ranking that separates solvents into three risk-based classes: class 1 having unacceptable toxicities, class 2 having less severe toxicity, and class 3 having low toxic potential.[27]

Based on the results, acetonitrile, isopropanol, 2-butanol, *n*-propanol, and (2 : 1) ethanol–water identified as having the

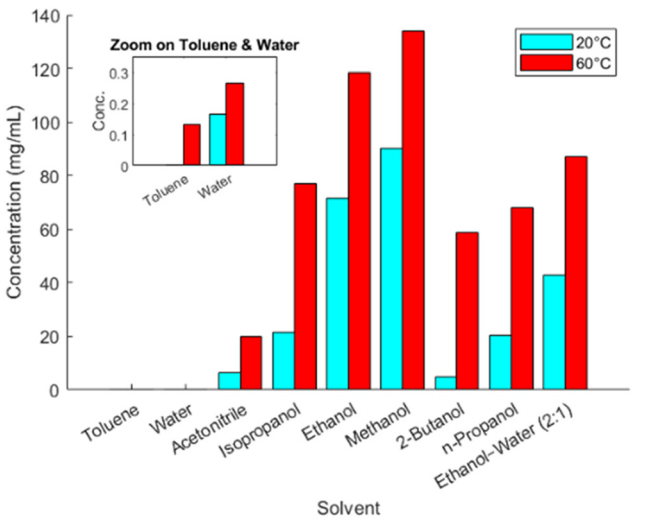

Fig. 2 Bar graph comparing the solubility of resveratrol in various solvent systems at 20 °C and 60 °C. Solubility values were determined experimentally and used to calculate the theoretical yield and assess the thermodynamic favorability of each solvent system within the KIT design framework. The inset highlights the low-solubility regime for both toluene and water systems to improve visual clarity.

Table 3 Summary of calculations from initial solubility data and chemical class

	Theoretical yield (%)	Solid concentration ($g_{solute}\ g_{solvent}^{-1}$)	*E*-Factor ($g_{solvent\ used}\ g_{solute\ produced}^{-1}$)	Class
Acetonitrile	67.3	1.71	58.44	Class 2
Isopropanol	71.9	7.06	14.17	Class 3
Ethanol	39.4	5.91	16.93	Class 3
Methanol	32.8	5.56	17.97	Class 2
2-Butanol	91.9	6.66	15.01	Class 3
n-Propanol	70.1	5.94	16.84	Class 3
Ethanol–water (2 : 1)	51.7	5.41	18.48	Class 3

highest theoretical yields and were selected for further investigation. Additional solubility data were collected at 10 °C intervals between 20 °C and 60 °C, and second-order polynomial models of the form from eqn (4) were fitted to the resulting data. The solubility curves are presented in Fig. 3, and the corresponding polynomial coefficients are provided in Table 4.

Following the determination of solubility curves, simple small-scale cooling crystallization experiments were performed to gain qualitative insight into the kinetic behavior of resveratrol in each solvent system. The focus was on assessing nucleation, growth, agglomeration, and crystal aspect ratio. Isopropanol, 2-butanol, and *n*-propanol did not exhibit primary nucleation, even when cooled to low temperatures and held for extended durations. To examine further, seed crystals were introduced to the system; however, no seed growth or secondary nucleation was observed, indicating poor kinetic suitability for crystallization.

These preliminary results narrowed down the feasible solvents to five: isopropanol–water, ethanol, methanol, acetonitrile, and ethanol–water. *In situ* images for these solvents were then used to qualitatively label their kinetic behavior as "high" or "low," as shown in Fig. 4. The isopropanol–water mixture, Fig. 4e, resulted in immediate and extensive agglomeration, thus making it unsuitable to move forward with. Ethanol and methanol, despite being common solvents for crystallization applications, exhibited low theoretical yield and unfavorable crystallization behavior, ethanol (Fig. 4b) showing poor growth tendencies and methanol (Fig. 4c) displaying significant agglomeration tendencies under simple cooling conditions, resulting in suboptimal crystalline products. Ultimately, only two solvent systems, acetonitrile and (2 : 1) ethanol–water, were feasible and displayed high nucleation and growth tendencies with minimal initial agglomeration. Acetonitrile (Fig. 4a) produced crystals with a low aspect ratio, while ethanol–water (Fig. 4e) led to high aspect ratio crystals. Both solvent systems were selected for further investigation in the subsequent studies.

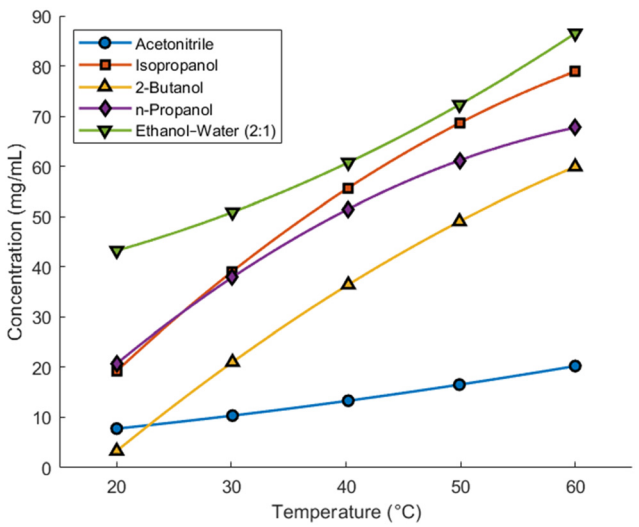

Fig. 3 Solubility curves of resveratrol in five solvent systems—acetonitrile, isopropanol, 2-butanol, *n*-propanol, and ethanol–water (2 : 1)—as a function of temperature. Experimental data are fitted with second-order polynomial equations to guide thermodynamic comparisons across solvents.

3.2. Characterization of resveratrol

During most experiments, an ultraviolet-visible (UV/vis) spectroscopy probe was used *in situ* to monitor the absorbance of resveratrol in solution over time. Spectral data were collected continuously, and the background absorbance from the corresponding solvent system was subtracted from each spectrum to isolate the signal belonging to resveratrol. An example of the spectra is shown in Fig. 5, demonstrating the evolution of absorbance during the experiment.

Raman spectroscopy was also employed to evaluate the final crystalline products for potential variation in solid-state form. Spectra from products crystallized in methanol, ethanol, and acetonitrile were compared to that of the resveratrol raw material. Representative spectra are shown in Fig. 6 and indicate no detectable differences between samples. Even crystals exhibiting very different morphologies, a common visual indication of potential polymorphism, produced identical

Table 4 Coefficients of selected second-order polynomial solubility curves

	a	*b*	*c*
Acetonitrile	0.00185	0.0164	3.724
Isopropanol	−0.0158	2.755	−29.526
2-Butanol	−0.0113	2.323	−38.648
n-Propanol	−0.0176	2.587	−23.972
Ethanol–water (2 : 1)	0.0108	0.215	34.602

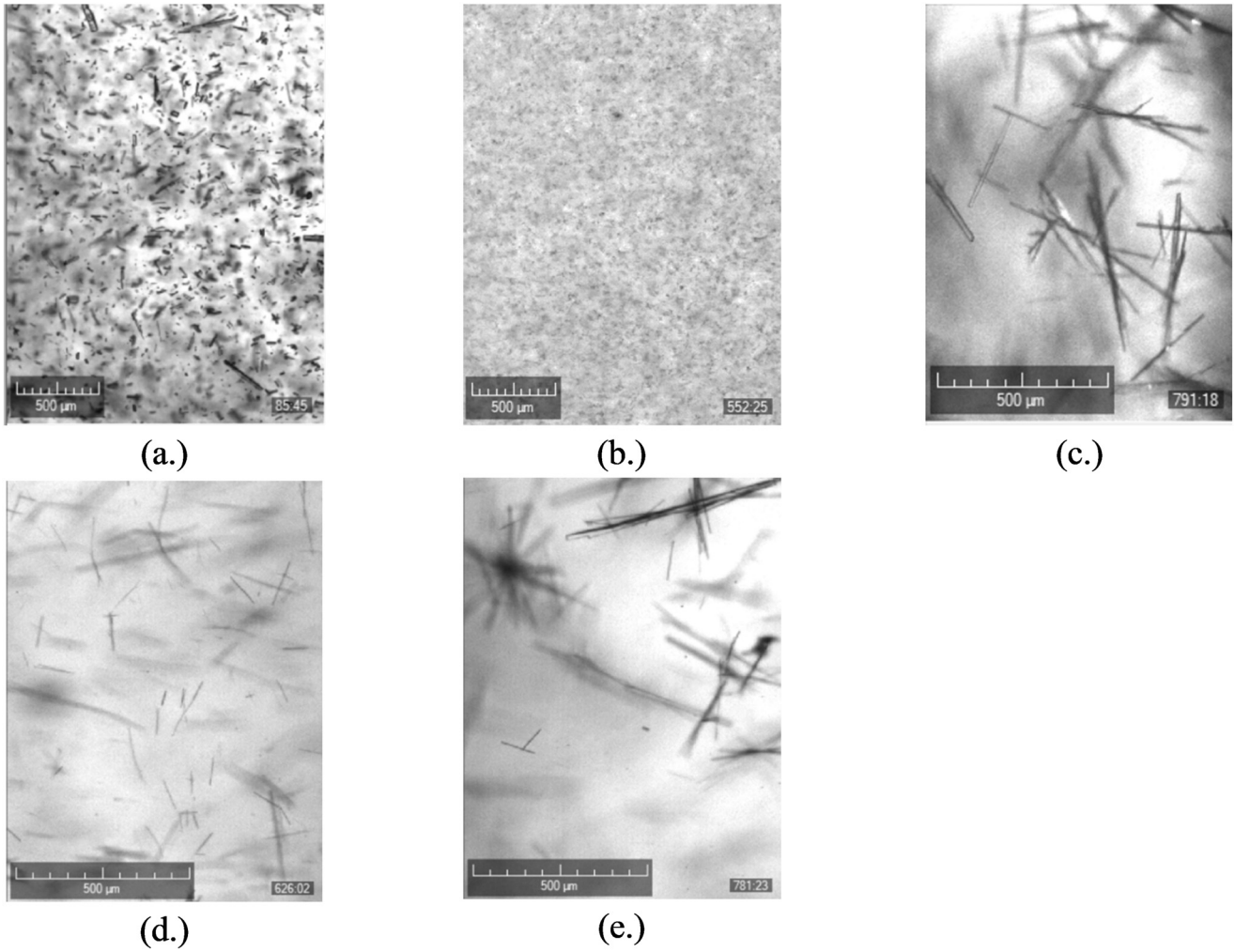

Fig. 4 Crystalline images of the five feasible solvents used to visually assess crystal product behavior: (a) acetonitrile, (b) ethanol, (c) methanol, (d) (2 : 1) ethanol–water, and (e) isopropanol–water.

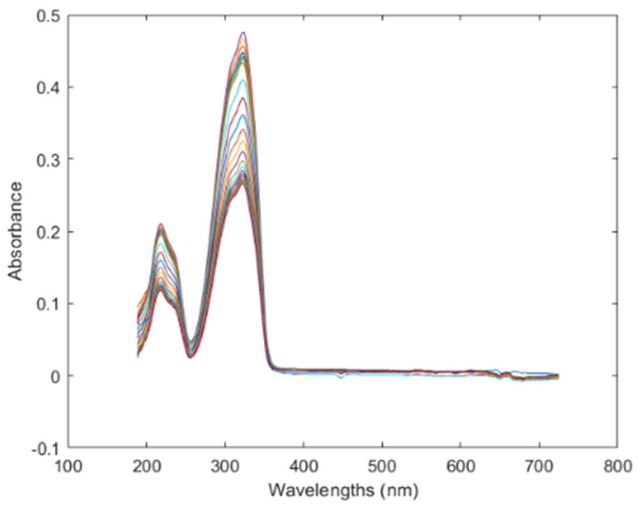

Fig. 5 Representative UV/vis absorbance spectrum of resveratrol in solution, with solvent background subtracted.

Raman spectra, suggesting that the shape differences were due to factors other than crystal structure. While Raman spectroscopy is sensitive to molecular conformation and hydrogen bonding, it was used here as a qualitative tool to assess sample consistency.

3.3. Crystallization in (2 : 1) ethanol–water

Cooling crystallization experiments for resveratrol in a (2 : 1 w/w) ethanol–water solvent system were run according to the design of experiments summarized in Table 1 and are shown in Fig. 7. The impact of operating conditions on crystal morphology was evident in both *in situ* and offline imaging. The final crystal product from experiment 2, which was unseeded and had a fast-cooling rate, is shown in Fig. 7b. The *in situ* image reveals a high population of very fine crystals that are difficult to distinguish individually due to their small size and overlap, indicating uncontrolled nucleation and rapid supersaturation depletion. In contrast, experiment 3, which involved 1 wt% seed under slow cooling

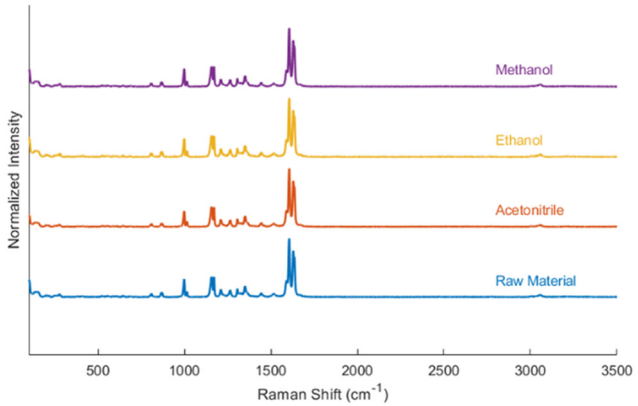

Fig. 6 Raman spectra of resveratrol crystallized from three different solvent systems (methanol, ethanol, acetonitrile, and raw material) under cooling crystallization conditions, compared to the purchased raw material. All spectra exhibit characteristic resveratrol peaks at ~1600 cm^{-1} and ~1630 cm^{-1}.

conditions, produced well-defined, high aspect ratio crystals with a pronounced needle-like morphology, as seen in Fig. 7e. These evident differences demonstrate the strong influence of operating conditions, particularly seeding and cooling rate, on the final crystal size and shape. These differences were further observed through offline imaging using a Teneo VolumeScope scanning electron microscope (SEM). After filtration and drying of the final slurries, SEM images of the collected crystal products were taken. Fig. 7c and f show the SEM images of experiments 2 and 3, respectively. In experiment 2, the product consists of very thin, plate-like crystals arranged in overlapping clusters likely due to the filtration and drying process. The SEM image of experiment 3 confirms the elongated, needle-like crystals consistent to what was observed *in situ*. These results further emphasize the need to carefully tune crystallization conditions to control particle attributes critical for downstream process performance. While only representative cases (experiments 2 and 3) are shown in Fig. 7, the remaining experiments (1, 4, 5, and 6) demonstrated crystal morphologies that align with expected trends based on their seed load and cooling rate combinations.

3.4. Crystallization in acetonitrile

Cooling crystallization experiments for resveratrol in acetonitrile were run under the operating conditions summarized in Table 1. The results from experiment 2, which was run at a fast-cooling rate of 0.5 °C min^{-1} and without seeding, are shown in Fig. 8a, where the temperature profile and FBRM total counts are plotted over time. The

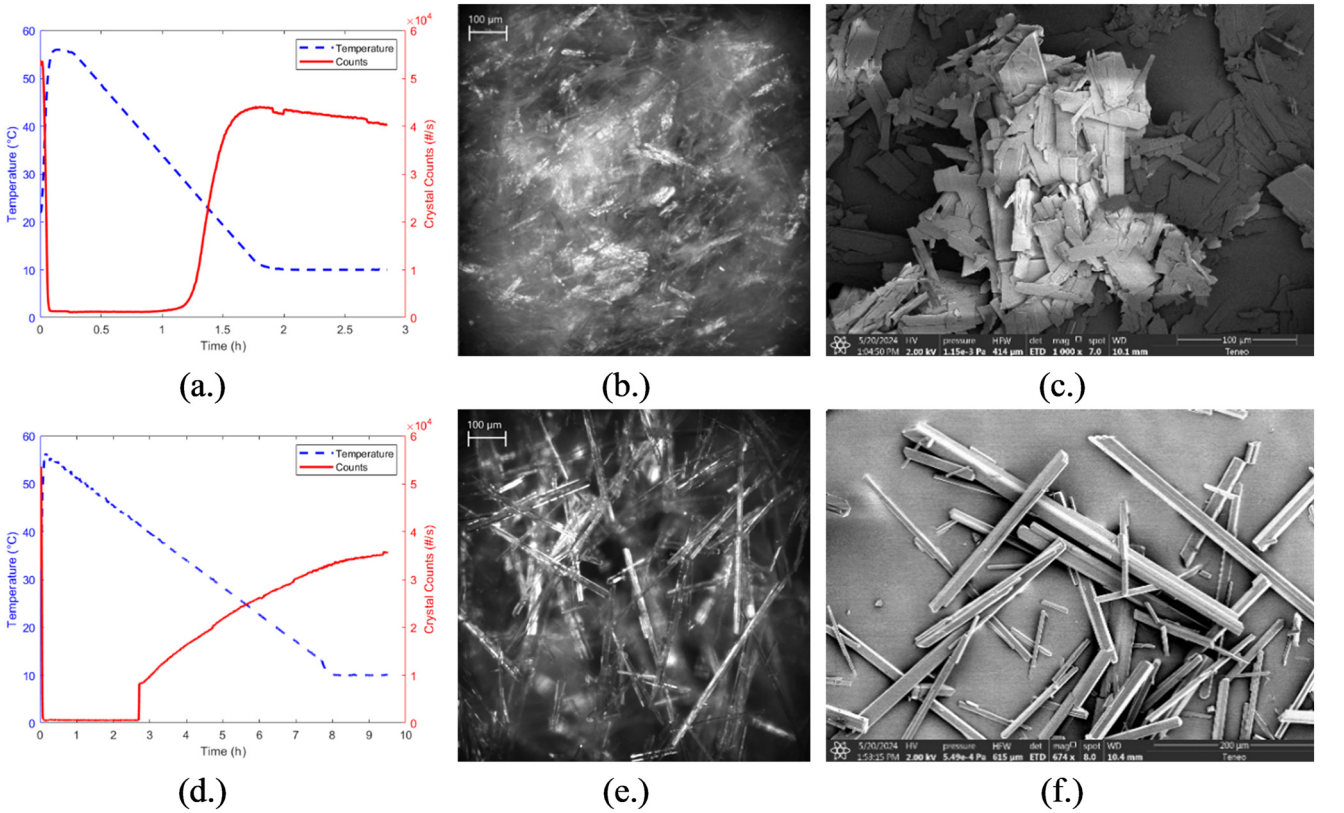

Fig. 7 Representative results from unseeded, fast cooling experiment (exp. 2) and 1 wt% seed, slow cool experiment (exp. 3) for reservatrol in ethanol–water (2 : 1). (a) Temperature and crystal count *versus* time for exp. 2. (b) *In situ* image of the final crystal product from exp. 2. (c) SEM image of the final crystal product from exp. 2. (d) Temperature and crystal count *versus* time for exp. 3. (e) *In situ* image of the final crystal product from exp. 3. (f) SEM image of the final crystal product from exp. 3.

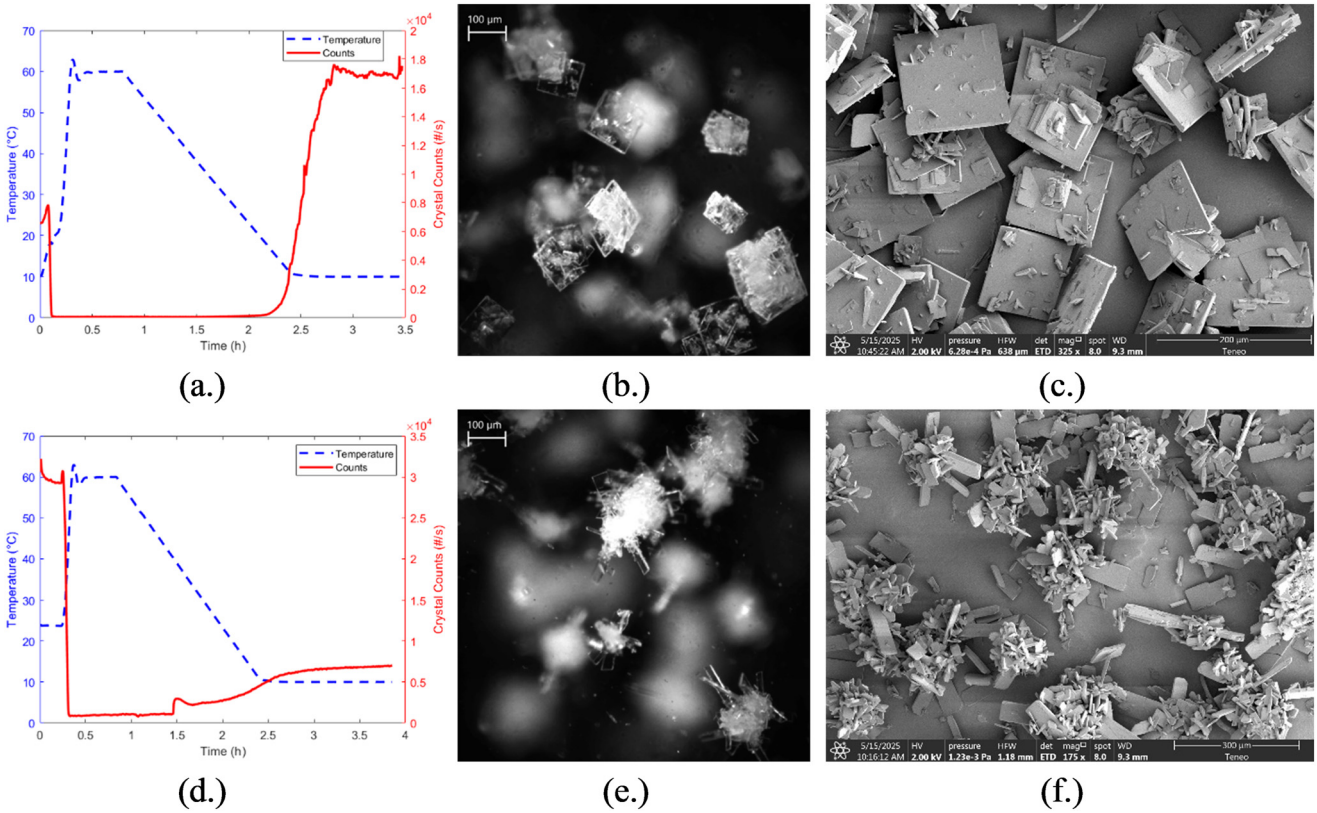

Fig. 8 Representative results from the unseeded, fast cooling experiment (exp. 2) and the 1 wt% seed, fast cooling experiment (exp. 4) for resveratrol in acetonitirile. (a) Temperature and crystal count *versus* time for exp. 2. (b) *In situ* image of the final crystal product from exp. 2. (c) SEM image of the final crystal product from exp. 2. (d) Temperature and crystal count *versus* time for exp. 4. (e) *In situ* image of the final crystal product from exp. 4. (f) SEM image of the final crystal product from exp. 4.

corresponding final crystal product, shown in Fig. 8b, was imaged using a Mettler-Toledo EasyViewer 100 and reveals crystals with a predominantly square-like morphology and relatively low aspect ratio. The crystals appear discrete and mildly agglomerated, revealing relatively controlled nucleation and growth behavior under these conditions. In contrast, experiment 4 (Fig. 8d), which was run at the same cooling rate but included 1 wt% seed addition, produced noticeably different results. As seen in Fig. 8e, the final crystal product displays elongated, high aspect ratio crystals with a significant degree of agglomeration and clustering. Many crystals appear to be intergrown with some crystals radiating outwards, which could indicate secondary nucleation effects. This morphological difference can be further seen in the SEM images, Fig. 8c and f, and it suggests that the presence of seed might have accelerated local supersaturation around the seed crystals, promoting uncontrolled growth or secondary nucleation. These results highlight the strong influence of seeding on crystal morphology and demonstrate how seeding strategies must be carefully optimized to avoid unfavorable particle formation. Again, only representative cases (experiments 2 and 4) are shown in Fig. 8, as they reflect the most extreme behaviors observed. The remaining experiments (1, 3, 5, and 6) followed the same trend: unseeded conditions resulted in minimal agglomeration, while seeded experiments consistently exhibited high agglomeration.

To evaluate the consistency of nucleation behavior under fast cooling and to define an appropriate target range for feedback control, a sequence of three crystallization experiments in acetonitrile was conducted: two fast linear cooling experiments followed by one direct nucleation control (DNC) experiment, Fig. 9. The two fast-cooling experiments were performed at a rate of 0.5 °C min^{-1} and compared based on FBRM total particle count values and *in situ* images obtained *via* the EasyViewer. In the first fast cooling run, the final crystal population reached around 9000 total counts and the product morphology appeared as small compact clusters, Fig. 9a. In contrast, the second fast cooling experiment resulted in a higher final particle count of 13 000, along with a square-like crystal morphology, Fig. 9b, like those observed in experiment 2. The variability in primary nucleation outcome—despite identical operating conditions—was consistently observed across fast-cooled runs and is likely related to the interplay between homogeneous and heterogeneous nucleation mechanisms. Based on these findings, the DNC experiment was designed with a lower target total count range (3600–5400) to promote larger crystal growth and minimize agglomeration. As cooling began, eventually particle counts increased, and once the counts exceeded 5400, the system switched to heating at +0.3 °C min^{-1} to dissolve fines

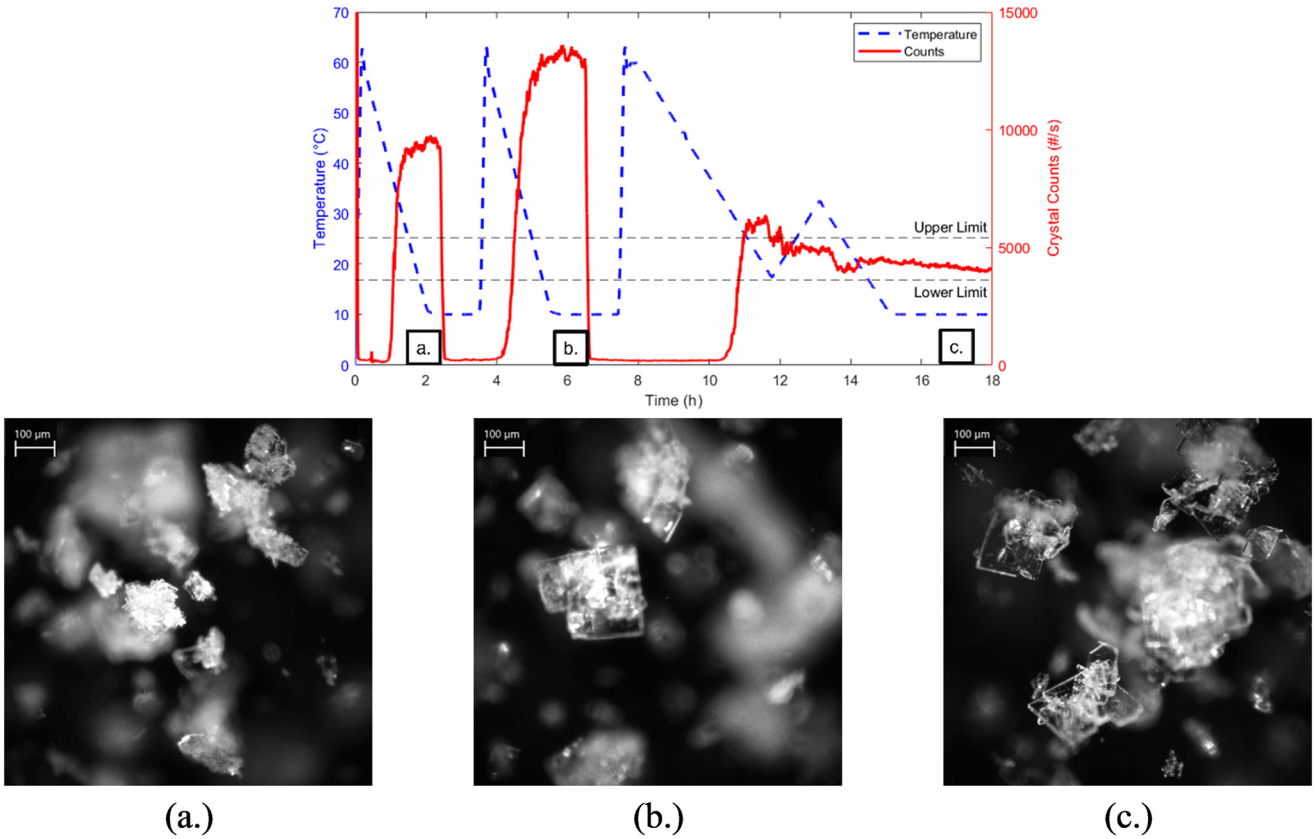

Fig. 9 Representative crystallization experiments illustrating temperature and crystal count profiles over time (top) and the corresponding final crystal products captured *via in situ* imaging (bottom). The time series plot includes three experiments: (a) fast cooling, (b) fast cooling, and (c) direct nucleation control (DNC) with a target range of 3600–5400 counts. Below each labeled point on the graph, the *in situ* images (a)–(c) show the resulting crystal morphology at the end of each respective experiment.

and smaller crystals, to reduce the particle population. Upon returning within the target range, cooling resumed at −0.3 °C min^{-1} until the final temperature of 10 °C was reached. This temperature-cycling behavior allowed the system to maintain nucleation control within the desired count window. The resulting crystal product, Fig. 9c, showed a slight increase in size compared to the fast cooling experiments. However, there was also a noticeable increase in agglomeration, suggesting that other strategies may be required to better manage the crystal size and aggregation.

Due to the significant variability observed in primary nucleation during the prior sequence of fast cooling, fast cooling, and DNC experiment, which resulted in substantial differences in crystal size, shape, and total particle counts, an additional DNC experiment was run, Fig. 10a. In this experiment, seed crystals were introduced to reduce the uncertainty associated with primary nucleation and to provide greater control over the process. The seeded DNC experiment was performed using a resveratrol acetonitrile solution, initially heated to 60 °C for complete dissolution. The system was then cooled at a rate of −0.3 °C min^{-1}, and at 40 °C, 1 wt% resveratrol seed was added. Cooling continued until the total particle counts exceeded the upper limit of 1600 counts, at which point the system switched to heating at +0.3 °C to dissolve fines and reduce the total crystal count. Once the count fell below the lower limit of 1200, cooling resumed until the final temperature of 10 °C was reached. At this point, the solution was held at this temperature since the counts were stable within the target range. The final crystal product, Fig. 10b and c, from this seeded DNC experiment demonstrated a significant increase in crystal size, with crystals reaching lengths of approximately 700 μm—the largest crystals observed from all acetonitrile experiments conducted. Morphologically, the crystals appeared well-defined and exhibited minimal agglomeration compared to prior fast-cooled or unseeded DNC runs. This outcome highlights the effectiveness of seeding combined with temperature cycling to manage nucleation and promote the growth of large, high-quality crystals. The success of this approach, seeded runs with a single temperature cycle, suggests that future batches could achieve similar outcomes without the need for feedback control. This approach not only improved crystal size and quality but also has the potential to enhance downstream filtration and drying efficiency.

3.5. Impact of the KIT approach

The KIT framework enabled rapid narrowing of viable solvent systems by coupling traditional thermodynamic

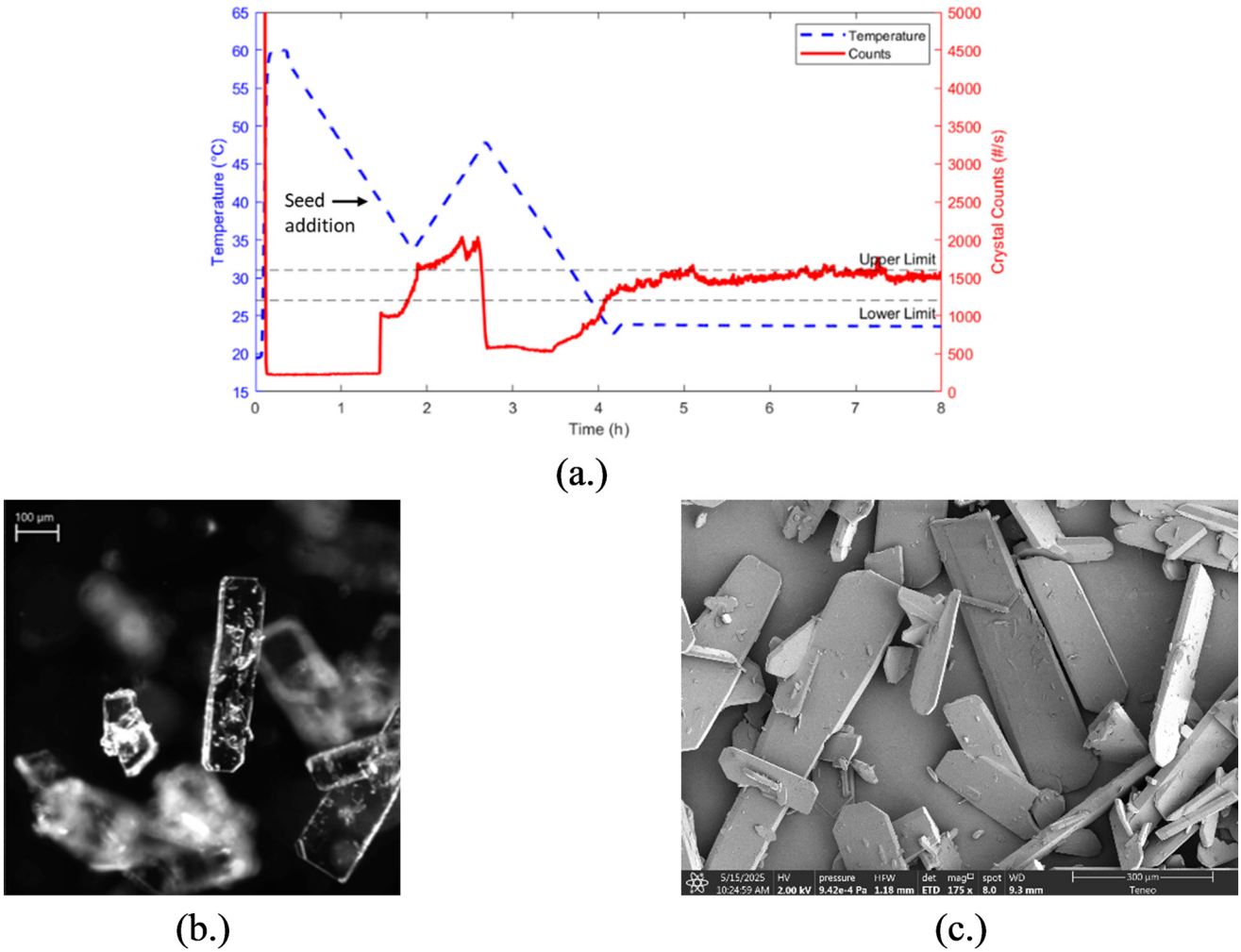

Fig. 10 Plot of temperature and crystal counts *versus* time (a) for the direct nucleation control experiment with 1 wt% seed with an upper limit of 1600 and a lower limit of 1200 counts, as well as two images of the final crystal product; (b) an *in situ* image and (c) an SEM image.

screening with early-stage kinetic evaluation. This dual-layered strategy revealed performance-limiting issues, such as low nucleation rates or agglomeration tendencies, that would not have been evident from solubility data alone. For instance, although isopropanol and methanol demonstrated acceptable solubility profiles, their poor nucleation or growth behavior led to their exclusion, streamlining the path to more promising candidates like acetonitrile and (2 : 1) ethanol–water. Moreover, KIT guided targeted process control strategies, such as seeding and temperature cycling in the DNC experiment, which significantly improved crystal quality and size. The outcome (large, well-defined crystals with reduced agglomeration) demonstrates how the KIT framework not only informs solvent selection but also directly enhances crystallization performance and process scalability. This proactive approach to solvent screening and process design lays a foundation for more robust and resource-efficient crystallization development in both research and industrial settings.

4. Conclusions

This study introduced a novel framework, the KIT design, for rapid yet robust solvent screening, demonstrated using the model compound resveratrol. By integrating traditional thermodynamic metrics (solubility, theoretical yield, and solid concentration) with simple yet insightful cooling crystallization experiments, the KIT design enabled a more holistic evaluation of solvent candidates. Key kinetic-based characteristics such as nucleation, growth, agglomeration, and aspect ratio were visually assessed and used to filter down an initial set of 19 solvent systems to five potential candidates: acetonitrile, ethanol, methanol, (2 : 1) ethanol–water, and isopropanol–water. Thermodynamic and kinetic considerations led to the elimination of ethanol and methanol (due to low theoretical yield and low nucleation/growth), and IPA–water (due to high agglomeration during initial cooling crystallization experiments), leaving (2 : 1) ethanol–water and acetonitrile as the most promising candidates. These two solvents were further explored through

a design of experiments to investigate the effects of cooling rate and seed loadings.

While the (2 : 1) ethanol–water system yielded high aspect ratio crystals under most conditions, the acetonitrile system initially resulted in very highly agglomerated crystals under seeded conditions. However, by applying direct nucleation control (DNC), first unseeded and then seeded, the agglomeration was reduced, and large crystals were obtained. While the framework does not eliminate kinetic hurdles entirely, it highlights them early and facilitates proactive management through experimental design and control strategies. Considering thermodynamic and kinetic crystallization characteristics, both acetonitrile (with control) and 2 : 1 ethanol–water (with minimal intervention) emerged as viable crystallization solvents for resveratrol. The KIT design approach not only improved solvent selection confidence but also demonstrated its potential to reduce development risk and guide smarter, more flexible process decisions.

Author contributions

Monika Neal: conceptualization, methodology, investigation, visualization, writing – original draft. Álmos Orosz: conceptualization, methodology, investigation, writing – review and editing. Rekha Rao: conceptualization, methodology, supervision, funding acquisition, project administration, writing – review and editing. Zoltan K. Nagy: conceptualization, methodology, investigation, supervision, funding acquisition, project administration, visualization, resources, writing – review and editing.

Conflicts of interest

None of the authors have a conflict of interest to disclose.

Data availability

The data used in this study are available on reasonable request from the corresponding author.

Acknowledgements

This work was supported by the Laboratory Directed Research and Development program at Sandia National Laboratories, a multi-mission laboratory managed and operated by National Technology and Engineering Solutions of Sandia LLC, a wholly owned subsidiary of Honeywell International Inc. for the U.S. Department of Energy's National Nuclear Security Administration under contract DE-NA0003525.

References

1 R. D. Braatz, *Annu. Rev. Control*, 2002, **26**, 87–99.
2 Z. K. Nagy, *Comput. Chem. Eng.*, 2009, **33**, 1685–1691.
3 A. Myerson, *Handbook of Industrial Crystallization*, Butterworth-Heinemann, 2002.
4 P. A. Larsen, D. B. Patience and J. B. Rawlings, *IEEE Control Syst. Mag.*, 2006, **26**, 70–80.
5 R. Parvaresh, S. Ferdoush, S. Kshirsagar, M. Gonzalez and Z. K. Nagy, *Cryst. Growth Des.*, 2024, **24**, 5355–5364.
6 A. Bártová, R. Gabriel, B. B. Prudilová, E. Otyepková, L. Malina and M. Otyepka, *Powder Technol.*, 2022, **402**, 117334.
7 S. Kshirsagar, B. Szilagyi and Z. K. Nagy, *Cryst. Growth Des.*, 2023, **23**(3), 1486–1499.
8 H. M. Omar and S. Rohani, *Cryst. Growth Des.*, 2017, **17**, 4028–4041.
9 C. Castagnoli, M. Yahyah, Z. Cimarosti and J. J. Peterson, *Org. Process Res. Dev.*, 2010, **14**, 1407–1419.
10 S. Daniel, Z. Kis, C. Kontoravdi and N. Shah, *Trends Biotechnol.*, 2022, **40**, 1213–1228.
11 B. Szilagyi and Z. K. Nagy, *Comput. Chem. Eng.*, 2019, **126**, 421–433.
12 F. Destro, Z. K. Nagy and M. Barolo, *Comput. Chem. Eng.*, 2022, **163**, 107809.
13 A. Eren, B. Szilágyi, J. Quon, M. Furuta, C. Papageorgiou and Z. K. Nagy, in *Computer Aided Chemical Engineering*, ed. A. A. Kiss, E. Zondervan, R. Lakerveld and L. Özkan, Elsevier, 2019, vol. 46, pp. 319–324.
14 W.-L. Wu, C. Chappelow, N. Hanspal, P. Larsen, J. Patton, A. Shinkle and Z. K. Nagy, *Ind. Eng. Chem. Res.*, 2022, **61**, 14561–14572.
15 A. Saleemi, C. Rielly and Z. K. Nagy, *CrystEngComm*, 2012, **14**, 2196–2203.
16 R. Parvaresh and Z. K. Nagy, *Ind. Eng. Chem. Res.*, 2025, **64**, 2858–2871.
17 Z. Gao, S. Rohani, J. Gong and J. Wang, *Engineering*, 2017, **3**, 343–353.
18 M. H. Muhieddine, S. K. Viswanath, A. Armstrong, A. Galindo and C. S. Adjiman, *Chem. Eng. Sci.*, 2022, **264**, 118125.
19 H. Kilari, I. Akturk, A. Tamas Csathy, M. Ekin Agca, U. Mathur and Z. K. Nagy, *CrystEngComm*, 2026, **28**, 812–835.
20 Á. Orosz, M. Neal, R. Rao, C. Roberts, B. Szilágyi and Z. K. Nagy, *AIChE J.*, 2025, **71**, e70094.
21 B. Salehi, A. P. Mishra, M. Nigam, B. Sener, M. Kilic, M. Sharifi-Rad, P. V. T. Fokou, N. Martins and J. Sharifi-Rad, *Biomedicines*, 2018, **6**, 91.
22 M. H. Keylor, B. S. Matsuura and C. R. J. Stephenson, *Chem. Rev.*, 2015, **115**, 8976–9027.
23 J. Orehek, D. Teslić and B. Likozar, *Org. Process Res. Dev.*, 2021, **25**, 16–42.
24 E. Simone, A. N. Saleemi, N. Tonnon and Z. K. Nagy, *Cryst. Growth Des.*, 2014, **14**, 1839–1850.
25 M. R. Abu Bakar, Z. K. Nagy, A. N. Saleemi and C. D. Rielly, *Cryst. Growth Des.*, 2009, **9**, 1378–1384.
26 E. Simone, W. Zhang and Z. K. Nagy, *Cryst. Growth Des.*, 2015, **15**, 2908–2919.
27 International Council for Harmonisation (ICH), Impurities: Guideline for Residual Solvents Q3C(R9), Step 5, January 2024.

